

Extraction of Dzyaloshinskii-Moriya interaction from propagating spin waves

Juriaan Lucassen ^{1,*}, Casper F. Schippers,¹ Marcel A. Verheijen,^{1,2} Patrizia Fritsch,³ Erik Jan Geluk,⁴ Beatriz Barcones,⁴ Rembert A. Duine,^{1,5} Sabine Wurmehl ^{3,6}, Henk J. M. Swagten,¹ Bert Koopmans,¹ and Reinoud Lavrijsen ^{1,†}

¹*Department of Applied Physics, Eindhoven University of Technology, P.O. Box 513, 5600 MB Eindhoven, Netherlands*

²*Eurofins Materials Science BV, High Tech Campus 11, 5656 AE Eindhoven, Netherlands*

³*IFW-Dresden, Institute for Solid State Research, Helmholtzstraße 20, 01069 Dresden, Germany*

⁴*NanoLab@TU/e, Eindhoven University of Technology, P.O. Box 513, 5600 MB Eindhoven, Netherlands*

⁵*Institute for Theoretical Physics, Utrecht University, Princetonplein 5, 3584 CC Utrecht, Netherlands*

⁶*Institute of Solid State and Materials Physics, TU Dresden, 01062 Dresden, Germany*



(Received 5 September 2019; revised manuscript received 13 December 2019; accepted 10 February 2020; published 28 February 2020)

The interfacial Dzyaloshinskii-Moriya interaction (iDMI) is of great interest in thin-film magnetism because of its ability to stabilize chiral spin textures. It can be quantified by investigating the frequency nonreciprocity of oppositely propagating spin waves. However, as the iDMI is an interface interaction, the relative effect reduces when the films become thicker, making quantification more difficult. Here, we utilize all-electrical propagating spin-wave spectroscopy to disentangle multiple contributions to spin wave frequency nonreciprocity to determine the iDMI. This is done by investigating nonreciprocities across a wide range of magnetic layer thicknesses (from 4 to 26 nm) in Pt/Co/Ir, Pt/Co/Pt, and Ir/Co/Pt stacks. We find the expected sign change in the iDMI when inverting the stack order and a negligible iDMI for the symmetric Pt/Co/Pt. We additionally extract a difference in surface anisotropies and find a large contribution due to the formation of different crystalline phases of the Co, which is corroborated using nuclear magnetic resonance and high-resolution transmission-electron-microscopy measurements. These insights will open up avenues to investigate, quantify, and disentangle the fundamental mechanisms governing the iDMI, and pave a way toward engineered large spin-wave nonreciprocities for magnonic applications.

DOI: [10.1103/PhysRevB.101.064432](https://doi.org/10.1103/PhysRevB.101.064432)

Within magnetism, the interfacial Dzyaloshinskii-Moriya interaction (iDMI) has gained enormous interest in recent years. It is an antisymmetric exchange interaction generated at symmetry-breaking interfaces with high spin-orbit coupling [1,2], which can stabilize noncollinear spin textures such as magnetic skyrmions [1–6]. Because of its importance in the field of noncollinear spin textures, it is vital to get a fundamental understanding of this interaction. For this, one requires methods that are able to accurately determine the iDMI [5,7–9]. We focus on spin-wave-based methods which rely on the iDMI-induced frequency difference between oppositely propagating spin waves, which is most commonly measured using the Brillouin Light Scattering (BLS) technique [10–15].

When it comes to quantifying iDMI, BLS is limited with respect to the frequency resolution, and is therefore only suited to reliably measure the iDMI in thin-film (~ 1 –2 nm) systems with a large iDMI to generate enough nonreciprocity [10–15]. Recently, all-electrical propagating spin-wave spectroscopy (PSWS) [16] has been proposed as an alternative for probing this frequency difference [12,17]. As this technique is more sensitive to small frequency differences (few MHz compared to tens to hundreds of MHz for BLS [18,19]), the lower bound of iDMI that can be quantified is significantly improved and allows for the nonreciprocity to be investigated

in thicker films (~ 20 nm), well beyond the thickness limit of BLS. For these thicker films, however, additional effects can play a role; for example, spin-wave localization in combination with a difference in interfacial anisotropy of the top and bottom interface can also lead to frequency differences between oppositely propagating spin waves [18].

In this paper, we therefore systematically untangle different contributions to the spin-wave frequency nonreciprocity utilizing PSWS to extract the iDMI. By investigating the nonreciprocity as a function of Co layer thickness t for Pt/Co/Ir, Pt/Co/Pt and Ir/Co/Pt systems we isolate the iDMI from other contributions to the nonreciprocity [18]. For Pt/Co/Ir and Ir/Co/Pt, we expect to find large but inverted DMI values, whilst the effective DMI for the symmetric Pt/Co/Pt should be small because the global symmetry is no longer broken [1,2,9]. This is indeed what we find for thin Co, where we also find the expected $1/t$ dependence of the nonreciprocity due to the interfacial nature of the iDMI. However, for thicker layers, the nonreciprocities are dramatically enhanced by a hitherto unconsidered effect; a change in the crystal phase of Co above a thickness of ~ 10 nm. Nevertheless, also in this regime the iDMI can be reliably extracted, further substantiating the powerful nature of PSWS to extract the iDMI over a large thickness range.

First, we demonstrate how spin-wave localization can also lead to a frequency nonreciprocity. This localization is a consequence of an asymmetry in the dynamic dipolar fields of a spin wave, which is illustrated in Fig. 1(a). In this figure,

*j.lucassen@tue.nl

†Corresponding author: r.lavrijsen@tue.nl

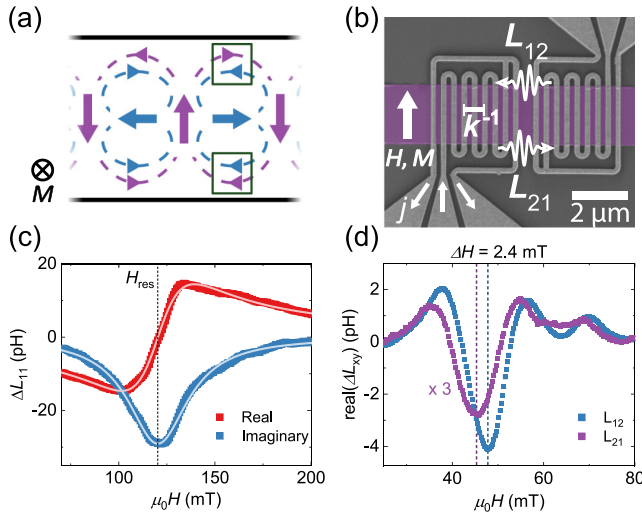


FIG. 1. (a) Schematic side view of a thin magnetic layer where the solid arrows indicate the dynamic components of the magnetization for a clockwise spin wave. The dashed lines are the resulting stray fields where the two boxes highlight the additive and destructive interference of the resulting stray fields at the bottom and top of the layer, respectively, leading to spin-wave localization. Adapted from Ref. [18]. (b) SEM micrograph of a fabricated device with $k = 8.5 \mu\text{m}^{-1}$. The magnetic strip is marked with a false color. We indicate the direction of the applied magnetic field H , current flow direction j , and the spin-wave flow direction given by the mutual inductions of the antennas (L_{xy}) and sign of k . (c) Self-induction ΔL_{11} as a function of applied magnetic field H measured at 15 GHz on Pt/Co(15)/Ir with $k = 7 \mu\text{m}^{-1}$. The dashed line indicates H_{res} extracted from the fit (solid lines). (d) Real part of the mutual-induction ΔL_{xy} (with a rescaled L_{21}) as a function of applied magnetic field H measured at 11 GHz on Pt/Co(12.3)/Ir with $k = 8.5 \mu\text{m}^{-1}$. The dashed lines demonstrate a measured peak shift ΔH of ~ 2.4 mT.

we show the dynamic components of the magnetization of a clockwise (CW) spin wave, including the resulting dipolar fields. As indicated with the boxes, these dipolar fields add up constructively at the bottom of the film and destructively near the top of the film. This asymmetry will localize the spin-wave on either the top or bottom interface, depending on the thickness of the magnetic film [18,20–22]. For a counterclockwise (CCW) spin wave, this localization is on the opposite surface. If the magnetic properties are asymmetric along the film thickness, this results in different resonance frequencies for the CW and CCW spin waves, which leads to a frequency nonreciprocity as CW and CCW waves travel in opposite directions. In this paper, this asymmetry results from asymmetries in the magnetic anisotropy across the bulk of the film.

A typical device used to measure these spin waves is shown in Fig. 1(b). Here two spin-wave antennas are placed on top of a magnetic strip. We drive an radio-frequency current through these antennas (whose spatial periodicity determines the spin-wave wave-vector k), which excites spin waves through its time-dependent Oersted fields. These spin waves then propagate to the second antenna, where they are detected via induction (L_{xy}). By inverting the detection and excitation antennas, we reverse the propagation direction of the detected spin waves. The magnetic strips consist of Ta(4)/X(4)/Co(t)/Y(3)/Pt(2), with (X,Y)=(Pt,Ir), (Ir,Pt), and

(Pt,Pt). We additionally varied the k vector from 4 to $10 \mu\text{m}^{-1}$ in $1.5 \mu\text{m}^{-1}$ increments by varying the antenna geometry, as described in Ref. [23].

We first investigate the self-induction L_{xx} of the antennas to extract the magnetic anisotropy. A typical measurement is shown in Fig. 1(c), where L_{11} is plotted as a function of the magnetic field H . This spectrum shows a typical FMR-like resonance profile indicative of spin-wave excitation. The real and imaginary parts are fitted simultaneously with a linear combination of a symmetric and antisymmetric Lorentzian line shape such that the resonance field H_{res} can be extracted (dashed line). Extracting the resonance fields for different frequencies and different t produces Fig. 2(a). Here, the resonance fields are fitted using well-known Kittel-like relations, with only the out-of-plane (OOP) anisotropy K as a fit parameter [24,25].¹

In Figs. 2(b)–2(d), we plot the fitted K as a function of t for the three different stacks. For all stacks, K decreases for increasing t when $t \lesssim 10$ nm. This is the interfacial anisotropy that reduces in magnitude due to the increasing magnetic volume. Above this thickness, we find that the anisotropy starts to increase again. This is attributed to a crystalline phase transition of the Co from face-centred cubic (fcc) to hexagonal close-packed (hcp) above a critical thickness t_{cr} , already widely observed in literature [26–31]. In the Supplemental Material [32], we confirm the presence of different structural phase contributions in films with different thicknesses using transmission electron microscopy (TEM) images and nuclear magnetic resonance (NMR) measurements. As the hcp phase has a much larger magnetocrystalline anisotropy along the c axis (OOP direction), this leads to an increase in K along the OOP direction [27]. Both OOP anisotropy contributions can be fitted simultaneously as

$$K = \begin{cases} \frac{K_s}{t} + K_{v,0} & t \leq t_{\text{cr}} \\ \frac{K_s}{t} + K_{v,0} + K_{v,1} \frac{t-t_{\text{cr}}}{t} & t > t_{\text{cr}}, \end{cases} \quad (1)$$

with $K_s = K_{s,\text{bot}} + K_{s,\text{top}}$ the total interfacial anisotropy, $K_{v,0}$ the crystalline anisotropy of the bottom half of the Co film, and $K_{v,1}$ the difference in the anisotropy between the top and bottom half of the film. This additional crystalline anisotropy is now included as a volume-weighted average through the last term, where we assume an fcc phase of thickness t_{cr} in the bottom half of the film, with the remainder of the Co film in the hcp phase [see inset Fig. 2(b)]. In Fig. 2(b), we fit the data to Eq. (1) and label the individual fitting parameters. The fits for the other two stacks are similarly plotted in Figs. 2(c)–2(d).

The resulting parameters from these fits are given in Table I. For the crystalline volume anisotropy terms, we find that there is quite a variation between the stacks. The variation in t_{cr} and K_v for Pt/Co/Ir and Pt/Co/Pt is hard to explain since both are grown on nominally identical underlayers. We tentatively attribute this to different growth conditions, as Pt/Co/Ir was grown in a different batch from Pt/Co/Pt and Ir/Co/Pt. Yet, the values for K_v are in line with literature,

¹With $M_s = 1.44 \text{ MA m}^{-1}$, $g = 2.17$, $k = 7 \mu\text{m}^{-1}$ (dictated by the antenna), and $w_{\text{eff}} = 1.2 \mu\text{m}$ [23].

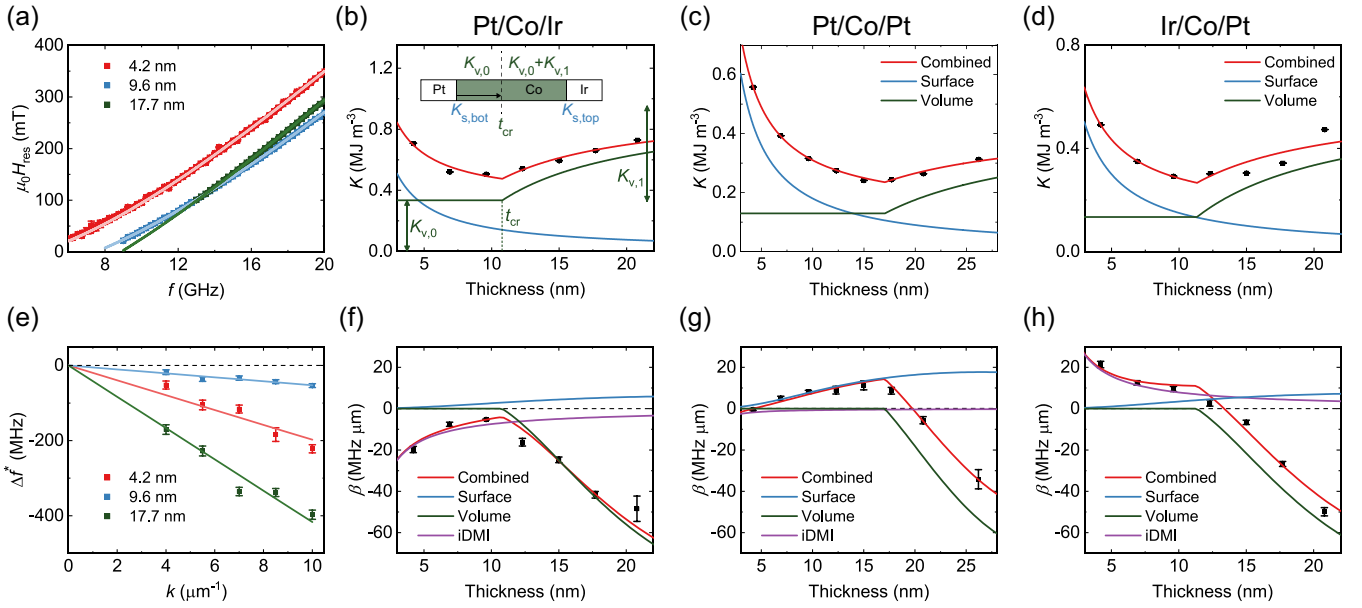


FIG. 2. (a) Fitted resonance fields H_{res} as a function of frequency f for Pt/Co(t)/Ir at different Co thicknesses t . (b)–(d) Anisotropy K as a function of Co thickness t for the three different stacks together with a fit that includes both a bulk and interfacial term which are plotted separately. The parameters that determine the bulk contribution ($K_{v,0}$, $K_{v,1}$ and t_{cr}) are labeled in (b). Inset of (b) shows a side view of the magnetic stack labeling the different anisotropy components. (e) Converted frequency shifts Δf^* as a function of wave vector k for Pt/Co(t)/Ir at different Co thicknesses t , including a linear fit through the origin. (f)–(h) Slope β of the wave vector dependence [extracted from linear fits; see (e)] as a function of layer thicknesses for the three different stacks. Also included is a fit that models this shift (combined) and the individual components (iDMI, surface, and volume) of that fit. For the fit parameters of (b)–(d) see Table I and for (f)–(h) see Table II.

where $K_{v,1} \approx 0.5 \text{ MJ m}^{-3}$ [27]. The values we find for t_{cr} are at least a factor 2–3 larger than those reported in literature for Pt/Co and Cu/Co systems. However, these details depend sensitively on the exact fabrication conditions [26,28–30].

With the anisotropy determined, we now shift our focus to the spin-wave transmission measurements to determine the frequency nonreciprocity. A typical transmission measurement of L_{xy} as function of magnetic field H is shown in Fig. 1(d). It shows a shift in resonance fields (dashed lines) ΔH between the oppositely propagating spin waves (L_{21} vs L_{12}) of about 2.4 mT^2 . This field shift is converted to a frequency shift Δf^* that is linear in k and (mostly) independent of the applied magnetic field when looking at shifts due to iDMI and ΔK_s [10,18]. Similar to how ferromagnetic resonance linewidths are converted, [42] we calculate $\Delta f^* = -(\frac{\partial H_{\text{res}}}{\partial f})^{-1} \Delta H$. These shifts are plotted as a function of k for arbitrary thicknesses in Fig. 2(e). For all measurements, the shifts are linear in k and the fitted slope β is used as a measure for the spin-wave frequency nonreciprocity.

As a final step in the analysis, in Fig. 2(f) we plot β as a function of layer thickness for Pt/Co/Ir. β is negative for all thicknesses and decreases as $\sim 1/t$ up to $t \approx 10 \text{ nm}$,

in agreement with an iDMI contribution that decreases with increasing thickness. We attribute the increase in β at $t = t_{\text{cr}}$ to the increase in crystalline anisotropy for $t > t_{\text{cr}}$. As the spin waves are localized at one of the two interfaces, the fact that the top part of the Co has a different crystalline volume anisotropy should indeed lead to a nonreciprocity, very similar to a nonreciprocity induced by a difference in surface anisotropies. In the Supplemental Material [32], we derive an analytical equation that we fit to β in Fig. 2(f). This fit contains three contributions: (i) the iDMI D_s which decreases as $1/t$, (ii) a surface contribution due to $\Delta K_s = K_{s,\text{bot}} - K_{s,\text{top}}$ which increases as t^2 [18], and (iii) the bulk volume contribution stemming from a different crystalline anisotropy above t_{cr} . Using the results from the fit of Fig. 2(b), the shifts were fitted with $K_{v,1}$, D_s , and ΔK_s as free parameters. As demonstrated in Fig. 2(f), there is an excellent agreement between the model and the measured shifts. Moreover, we find that the shift is dominated by the iDMI below t_{cr} and by the volume term due to the crystal phase transition above t_{cr} . This is in contrast to literature, where a nonreciprocity at higher thicknesses is usually ascribed to differences in surface anisotropies

TABLE I. Fit parameters of the fits of the anisotropy for the different stacks displayed in Figs. 2(b)–2(d). They include the surface anisotropy K_s and the three volume anisotropy terms indicated in Eq. (1).

	K_s (mJ m ⁻²)	$K_{v,0}$ (MJ m ⁻³)	$K_{v,1}$ (MJ m ⁻³)	t_{cr} (nm)
Pt/Co/Ir	1.5 ± 0.3	0.33 ± 0.05	0.63 ± 0.07	10.8 ± 0.6
Pt/Co/Pt	1.80 ± 0.02	0.130 ± 0.004	0.31 ± 0.06	17.0 ± 0.5
Ir/Co/Pt	1.5 ± 0.2	0.13 ± 0.04	0.5 ± 0.1	11.3 ± 0.9

²The shifts are determined using individual cross-correlations of the real and imaginary parts of L_{12} with L_{21} . They are then averaged with the negative shifts at negative fields to remove any biases. A method where we fit the actual peak locations was also used and yielded similar shifts (see the Supplemental Material [32]). Some additional considerations on shift extraction are also presented in the Supplemental Material [32].

TABLE II. Fit parameters from the fits of the slopes of the shifts for the different stacks shown in Figs. 2(f)–2(h). They include the terms that induce a shift, which is the increase in volume anisotropy $K_{v,1}$ above t_{cr} , the iDMI D_s , and difference in surface anisotropies $\Delta K_s = K_{s,bot} - K_{s,top}$. The last two columns use K_s from Table I and combines it with ΔK_s to calculate the interfacial anisotropies at the bottom and top interfaces.

	$K_{v,1}$ (MJ m ⁻³)	D_s (pJ m ⁻¹)	ΔK_s (mJ m ⁻²)	$K_{s,bot}$ (mJ m ⁻²)	$K_{s,top}$ (mJ m ⁻²)
Pt/Co/Ir	0.30 ± 0.03	-1.0 ± 0.2	0.2 ± 0.1	0.9 ± 0.2	0.7 ± 0.2
Pt/Co/Pt	0.25 ± 0.04	-0.10 ± 0.04	0.66 ± 0.06	1.23 ± 0.03	0.57 ± 0.03
Ir/Co/Pt	0.32 ± 0.04	1.0 ± 0.2	0.3 ± 0.2	0.9 ± 0.1	0.6 ± 0.2

[12,18]. The slopes β and corresponding fits for Pt/Co/Pt and Ir/Co/Pt are shown in Figs. 2(g) and 2(h) and the resulting fit parameters of the shifts are displayed in Table II.

With these results, we make three observations. First, there is the expected behavior of the effective iDMI, which changes sign upon stack reversal between Pt/Co/Ir and Ir/Co/Pt. Moreover, for the nominally symmetric Pt/Co/Pt stack, the iDMI is heavily reduced, as expected, because the global inversion symmetry is no longer broken [1,2]. From literature, the sign of the iDMI at the Pt/Co interface is well known, but there is still intense debate about the sign of the iDMI at the Ir/Co interface [43]. Because the iDMI in the Pt/Co/Ir stack is enhanced with respect to Pt/Co/Pt, we know the iDMI at the Ir/Co interface is either much smaller and/or has the opposite sign with respect to a Pt/Co interface. Additionally, the negligible DMI of the Pt/Co/Pt stack indicates that the DMI at the Pt/Co and Co/Pt interface is almost equal. Combining this with an iDMI for Pt/Co/Ir and Ir/Co/Pt that is smaller than the expected DMI at the Pt/Co interface of ≈ -1.5 pJ m⁻¹ [9] suggests that in our system the sign at the Ir/Co interface is the same as that of the Pt/Co interface [43].

Second, the differences in surface anisotropies are of the same sign such that the bottom interface always has a higher anisotropy than the top interface. The last two columns in Table II calculate the corresponding interfacial terms, where we find that the Pt/Co and Ir/Co interfaces have approximately the same interfacial anisotropy, but that the bottom surface always has a higher anisotropy compared to the corresponding top interface, confirming earlier conjectures [44,45]. If we assume that both the anisotropy and iDMI depend in a similar manner on the interfacial quality, we can extrapolate the ratio between $K_{s,bot/top}$ to the iDMI for Pt/Co/Pt. This gives an iDMI at the bottom Pt/Co interface of about -0.2 pJ m⁻¹. As this is significantly lower than what is reported (-1.5 pJ m⁻¹ [9]), it suggests that the iDMI and anisotropy do not depend in a similar manner on the interfacial quality.

Last, the values for $K_{v,1}$ (Table II) can vary by a factor of 2 from the results of the anisotropy fits (Table I). The TEM and NMR data show a gradual transition between the fcc and hcp phases as a function of thickness. In contrast, the assumed anisotropy profile [Eq. (1)] describes an instantaneous transition from fcc to hcp at t_{cr} . This oversimplification in the fits could potentially explain the different $K_{v,1}$ values.

We have shown that PSWS can be used to extract the different contributions to the frequency nonreciprocity over a wide thickness range. This makes it an extremely powerful tool for fundamental investigations into the DMI. For example, there is great interest in the manipulation of the iDMI via an electric field (EF) [46]. PSWS should prove very

powerful in quantifying the effect of the EF on the DMI [12], as it is able to separate the EF effect on the iDMI from the EF effect on the anisotropy. The latter is known to be present and, as we demonstrate, cannot be ignored when interpreting the frequency nonreciprocity to extract the iDMI [47]. The additional effects demonstrated here could also explain some of the puzzling behavior in Ref. [12]. Here, PSWS was used to measure the iDMI-induced shift in thick Pt/Co/MgO films which seem to be of the wrong sign and significantly larger than reported elsewhere in literature [9,12–15].

The large nonreciprocity demonstrated in this paper, induced by the crystalline phase change, can also be used in the field of magnonics. Different types of (proposed) devices rely extensively on spin-wave nonreciprocity [48–51]. Although iDMI can enhance this nonreciprocity [9,12–15], the thin films required to generate large nonreciprocities usually have large damping and low spin-wave group velocities. Rather, this work suggests that using crystalline anisotropies might offer a significantly more practical route toward increasing the spin-wave nonreciprocity. Although the system investigated here relies on a strain-induced crystalline phase transition that can be impractical, more feasible routes can be imagined; for instance, using a bilayer of fcc Co and [Co/Ni] repeats [52] to act as the low and high anisotropy materials, respectively. This additionally leads to a naturally occurring magnetization gradient across the thickness, further enhancing the frequency nonreciprocity [53].

Summarizing, we have shown in this paper that the physics behind spin-wave frequency nonreciprocity is more complex than originally assumed and includes a yet unnoticed but important contribution that is the result of a change in structural phase as function of film thickness. However, by investigating the thickness dependence of the nonreciprocity, we can uniquely isolate the iDMI, the difference in interfacial anisotropies, and a large contribution induced by this crystalline phase transition.

ACKNOWLEDGMENTS

This work is part of the research program of the Foundation for Fundamental Research on Matter (FOM), which is part of the Netherlands Organisation for Scientific Research (NWO). Solliance and the Dutch province of Noord-Brabant are acknowledged for funding the TEM facility. Financial support is acknowledged from the Deutsche Forschungsgemeinschaft (DFG) through Grants No. WU595/3-3 and No. WU595/14-1. This work is also supported in part by the European Research Council via Consolidator Grant number 725509 SPINBEYOND. We also thank V. Vandalon for help with the quantitative TEM analysis.

- [1] M. Heide, G. Bihlmayer, and S. Blügel, *Phys. Rev. B* **78**, 140403(R) (2008).
- [2] A. N. Bogdanov and U. K. Röbber, *Phys. Rev. Lett.* **87**, 037203 (2001).
- [3] M. Bode, M. Heide, K. von Bergmann, P. Ferriani, S. Heinze, G. Bihlmayer, A. Kubetzka, O. Pietzsch, S. Blügel, and R. Wiesendanger, *Nature* **447**, 190 (2007).
- [4] S. Emori, U. Bauer, S.-M. Ahn, E. Martinez, and G. S. D. Beach, *Nat. Mater.* **12**, 611 (2013).
- [5] K.-S. Ryu, L. Thomas, S.-H. Yang, and S. Parkin, *Nat. Nanotechnol.* **8**, 527 (2013).
- [6] A. Fert, V. Cros, and J. Sampaio, *Nat. Nanotechnol.* **8**, 152 (2013).
- [7] S.-G. Je, D.-H. Kim, S.-C. Yoo, B.-C. Min, K.-J. Lee, and S.-B. Choe, *Phys. Rev. B* **88**, 214401 (2013).
- [8] C.-F. Pai, M. Mann, A. J. Tan, and G. S. D. Beach, *Phys. Rev. B* **93**, 144409 (2016).
- [9] D.-S. Han, N.-H. Kim, J.-S. Kim, Y. Yin, J.-W. Koo, J. Cho, S. Lee, M. Kläui, H. J. M. Swagten, B. Koopmans, and C.-Y. You, *Nano Lett.* **16**, 4438 (2016).
- [10] J.-H. Moon, S.-M. Seo, K.-J. Lee, K.-W. Kim, J. Ryu, H.-W. Lee, R. D. McMichael, and M. D. Stiles, *Phys. Rev. B* **88**, 184404 (2013).
- [11] D. Cortés-Ortuño and P. Landeros, *J. Phy.-Condens. Mat.* **25**, 156001 (2013).
- [12] J. M. Lee, C. Jang, B.-C. Min, S.-W. Lee, K.-J. Lee, and J. Chang, *Nano Lett.* **16**, 62 (2016).
- [13] H. T. Nembach, J. M. Shaw, M. Weiler, E. Jué, and T. J. Silva, *Nat. Phys.* **11**, 825 (2015).
- [14] J. Cho, N.-H. Kim, S. Lee, J.-S. Kim, R. Lavrijsen, A. Solignac, Y. Yin, D.-S. Han, N. J. J. van Hoof, H. J. M. Swagten, B. Koopmans, and C.-Y. You, *Nat. Commun.* **6**, 7635 (2015).
- [15] K. Di, V. L. Zhang, H. S. Lim, S. C. Ng, M. H. Kuok, J. Yu, J. Yoon, X. Qiu, and H. Yang, *Phys. Rev. Lett.* **114**, 047201 (2015).
- [16] V. Vlaininck and M. Bailleul, *Science* **322**, 410 (2008).
- [17] S. Seki, Y. Okamura, K. Kondou, K. Shibata, M. Kubota, R. Takagi, F. Kagawa, M. Kawasaki, G. Tatara, Y. Otani, and Y. Tokura, *Phys. Rev. B* **93**, 235131 (2016).
- [18] O. Gladii, M. Haidar, Y. Henry, M. Kostylev, and M. Bailleul, *Phys. Rev. B* **93**, 054430 (2016).
- [19] T. Sebastian, K. Schultheiss, B. Obry, B. Hillebrands, and H. Schultheiss, *Front. Phys.* **3**, 35 (2015).
- [20] R. Damon and J. Eshbach, *J. Phys. Chem. Solids* **19**, 308 (1961).
- [21] D. D. Stancil and A. Prabhakar, Magnetostatic modes, in *Spin Waves: Theory and Applications* (Springer US, Boston, MA, 2009), pp. 139–168.
- [22] M. Kostylev, *J. Appl. Phys.* **113**, 053907 (2013).
- [23] J. Lucassen, C. F. Schippers, L. Rutten, R. A. Duine, H. J. M. Swagten, B. Koopmans, and R. Lavrijsen, *Appl. Phys. Lett.* **115**, 012403 (2019).
- [24] B. A. Kalinikos and A. N. Slavin, *J. Phys. C. Solid State* **19**, 7013 (1986).
- [25] B. A. Kalinikos, *Sov. Phys. J.* **24**, 718 (1981).
- [26] P. Riedi, T. Thomson, and G. Tomka, in *Handbook of Magnetic Materials*, Vol. 12 (Elsevier, Amsterdam, 1999), Chap. 2, pp. 97–258.
- [27] M. T. Johnson, P. J. H. Bloemen, F. J. A. den Broeder, and J. J. de Vries, *Rep. Prog. Phys.* **59**, 1409 (1996).
- [28] M. Tokaç, S. A. Bunyayev, G. N. Kakazei, D. S. Schmool, D. Atkinson, and A. T. Hindmarch, *Phys. Rev. Lett.* **115**, 056601 (2015).
- [29] N. Nakajima, T. Koide, T. Shidara, H. Miyauchi, H. Fukutani, A. Fujimori, K. Iio, T. Katayama, M. Nývlt, and Y. Suzuki, *Phys. Rev. Lett.* **81**, 5229 (1998).
- [30] D. Weller, A. Carl, R. Savoy, T. Huang, M. Toney, and C. Chappert, *J. Phys. Chem. Solids* **56**, 1563 (1995).
- [31] M. L. M. Laliou, R. Lavrijsen, R. A. Duine, and B. Koopmans, *Phys. Rev. B* **99**, 184439 (2019).
- [32] See Supplemental Material at <http://link.aps.org/supplemental/10.1103/PhysRevB.101.064432> for (i) frequency dependence of the shifts, (ii) a different method to determine the non-reciprocities, (iii) NMR data, (iv) TEM data, and (v) an analytical derivation of the shift. It additionally includes Refs. [33–41].
- [33] P. Bryant and H. Suhl, *Appl. Phys. Lett.* **54**, 2224 (1989).
- [34] M. Bailleul, D. Olligs, and C. Fermon, *Phys. Rev. Lett.* **91**, 137204 (2003).
- [35] P. Panissod, in *NATO ASI Series High Tech*, Vol. 48, edited by V. G. Baryakhtar, P. E. Wigen, and N. A. Lesnik (Kluwer Academic, Dordrecht, 1997), p. 225.
- [36] G. J. Strijkers, J. T. Kohlhepp, H. J. M. Swagten, and W. J. M. de Jonge, *Appl. Magn. Reson.* **19**, 461 (2000).
- [37] H. Wieldraaijer, W. J. M. de Jonge, and J. T. Kohlhepp, *Phys. Rev. B* **72**, 155409 (2005).
- [38] H. Wieldraaijer, W. J. M. de Jonge, and J. T. Kohlhepp, *J. Magn. Mater.* **286**, 390 (2005).
- [39] S. Wurmehl and J. T. Kohlhepp, *J. Phys. D* **41**, 173002 (2008).
- [40] H. A. M. de Gronckel, C. H. W. Swüste, K. Kopinga, and W. J. M. de Jonge, *Appl. Phys. A* **49**, 467 (1989).
- [41] J. W. Edington, Electron diffraction in the electron microscope, in *Electron Diffraction in the Electron Microscope* (Macmillan Education UK, London, 1975), pp. 1–77.
- [42] S. S. Kalarickal, P. Krivosik, M. Wu, C. E. Patton, M. L. Schneider, P. Kabos, T. J. Silva, and J. P. Nibarger, *J. Appl. Phys.* **99**, 093909 (2006).
- [43] F. Kloodt-Twesten, S. Kuhrau, H. P. Oepen, and R. Frömter, *Phys. Rev. B* **100**, 100402(R) (2019).
- [44] R. Lavrijsen, D. M. F. Hartmann, A. van den Brink, Y. Yin, B. Barcones, R. A. Duine, M. A. Verheijen, H. J. M. Swagten, and B. Koopmans, *Phys. Rev. B* **91**, 104414 (2015).
- [45] S. Bandiera, R. C. Sousa, B. Rodmacq, and B. Dieny, *IEEE Magn. Lett.* **2**, 3000504 (2011).
- [46] T. Srivastava, M. Schott, R. Juge, V. Krizáková, M. Belmeguenai, Y. Roussigné, A. Bernand-Mantel, L. Ranno, S. Pizzini, S.-M. Chérif, A. Stashkevich, S. Auffret, O. Boulle, G. Gaudin, M. Chshiev, C. Baraduc, and H. Béa, *Nano Lett.* **18**, 4871 (2018); W. Zhang, H. Zhong, R. Zang, Y. Zhang, S. Yu, G. Han, G. L. Liu, S. S. Yan, S. Kang, and L. M. Mei, *Appl. Phys. Lett.* **113**, 122406 (2018); K. Nawaoka, S. Miwa, Y. Shiota, N. Mizuoichi, and Y. Suzuki, *Appl. Phys. Express* **8**, 063004 (2015).
- [47] See for example B. Rana and Y. Otani, *Comm. Phys.* **2**, 90 (2019) and references therein.
- [48] R. Camley, *Surf. Sci. Rep.* **7**, 103 (1987).
- [49] J.-V. Kim, R. L. Stamps, and R. E. Camley, *Phys. Rev. Lett.* **117**, 197204 (2016).

- [50] R. Verba, V. Tiberkevich, E. Bankowski, T. Meitzler, G. Melkov, and A. Slavin, *Appl. Phys. Lett.* **103**, 082407 (2013).
- [51] M. Jamali, J. H. Kwon, S.-M. Seo, K.-J. Lee, and H. Yang, *Sci. Rep.* **3**, 3160 (2013).
- [52] M. Arora, R. Hübner, D. Suess, B. Heinrich, and E. Girt, *Phys. Rev. B* **96**, 024401 (2017).
- [53] R. A. Gallardo, P. Alvarado-Seguel, T. Schneider, C. Gonzalez-Fuentes, A. Roldán-Molina, K. Lenz, J. Lindner, and P. Landeros, *New J. Phys.* **21**, 033026 (2019).